# Prevalence of Bimolecular Routes in the Activation of Diatomic Molecules with Strong Chemical Bonds (O$_2$, NO, CO, N$_2$) on Catalytic Surfaces

David Hibbitts and Enrique Iglesia*

Department of Chemical and Biomolecular Engineering, University of California, Berkeley, California 94720, United States

**CONSPECTUS:** Dissociation of the strong bonds in O$_2$, NO, CO, and N$_2$ often involves large activation barriers on low-index planes of metal particles used as catalysts. These kinetic hurdles reflect the noble nature of some metals (O$_2$ activation on Au), the high coverages of co-reactants (O$_2$ activation during CO oxidation on Pt), or the strength of the chemical bonds (NO on Pt, CO and N$_2$ on Ru). High barriers for direct dissociations from density functional theory (DFT) have led to a consensus that "defects", consisting of low-coordination exposed atoms, are required to cleave such bonds, as calculated by theory and experiments for model surfaces at low coverages. Such sites, however, bind intermediates strongly, rendering them unreactive at the high coverages prevalent during catalysis. Such site requirements are also



at odds with turnover rates that often depend weakly on cluster size or are actually higher on larger clusters, even though defects, such as corners and edges, are most abundant on small clusters. This Account illustrates how these apparent inconsistencies are resolved through activations of strong bonds assisted by co-adsorbates on crowded low-index surfaces.

Catalytic oxidations occur on Au clusters at low temperatures in spite of large activation barriers for O$_2$ dissociation on Au(111) surfaces, leading to proposals that O$_2$ activation requires low-coordination Au atoms or Au-support interfaces. When H$_2$O is present, however, O$_2$ dissociation proceeds with low barriers on Au(111) because chemisorbed peroxides (*OOH* and *HOOH*) form and weaken O−O bonds before cleavage, thus allowing activation on low-index planes. DFT-derived O$_2$ dissociation barriers are much lower on bare Pt surfaces, but such surfaces are nearly saturated with CO* during CO oxidation. A dearth of vacant sites causes O$_2$* to react with CO* to form *OOCO* intermediates that undergo O−O cleavage. NO-H$_2$ reactions occur on Pt clusters saturated with NO* and H*; direct NO* dissociation requires vacant sites that are scarce on such surfaces. N−O bonds cleave instead via H*-assistance to form *HNOH* intermediates, with barriers much lower than for direct NO* dissociation. CO hydrogenation on Co and Ru occurs on crowded surfaces saturated with CO*; rates increase with increasing Co and Ru cluster size, indicating that low-index surfaces on large clusters can activate CO*. Direct CO* dissociation, however, occurs with high activation barriers on low-index Co and Ru surfaces, and even on defect sites (step-edge, corner sites) at high CO* coverages. CO* dissociation proceeds instead with H*-assistance to form *HCOH* species that cleave C−O bonds with lower barriers than direct CO* dissociation, irrespective of surface coordination. H$_2$O increases CO activation rates by assisting H-additions to form *HCOH*, as in the case of peroxide formation in Au-catalyzed oxidations. N$_2$ dissociation steps in NH$_3$ synthesis on Ru and Fe are thought to also require defect sites; yet, barriers on Ru(0001) indicate that H*-assisted N$_2$ activation − unlike O$_2$, CO, and NO − is not significantly more facile than direct N$_2$ dissociation, suggesting that defects and low-index planes may both contribute to NH$_3$ synthesis rates.

The activation of strong chemical bonds often occurs via bimolecular reactions. These steps weaken such bonds before cleavage on crowded low-index surfaces, thus avoiding the ubiquitous kinetic hurdles of direct dissociations without requiring defect sites.
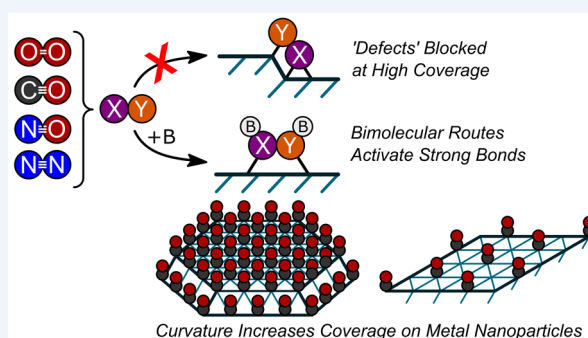
## INTRODUCTION

Low-index planes of noble metal surfaces are often unable to activate diatomic molecules containing double or triple bonds, such as O$_2$, NO, N$_2$, and CO (in order of increasing bond dissociation energies (BDE)),[1] via direct interactions with ensembles of bare metal atoms. Bare Au(111) surfaces do not even activate O$_2$ (weakest bond among these molecules[1]);[2,3] such kinetic hurdles have led to proposals indicating O$_2$ dissociation occurs on low-coordination sites at edges or corners of Au nanoparticles,[2−4] or at atomic contacts between

Au clusters and reducible oxides.[4−6] Bare Pt(111) surfaces, in contrast, dissociate O$_2$ with low activation barriers, but become saturated with chemisorbed CO (CO*) during CO oxidation; in such cases, a dearth of vacant sites and strong adsorbate−adsorbate interactions render any exposed Pt atoms less reactive (more noble) by a combination of electronic and steric effects, leading to higher barriers and lower O$_2$

dissociation rates than on bare Pt surfaces.[7,8] Even surfaces of less noble metals, such as Co(0001)[9] and Ru(0001),[10] exhibit high CO dissociation barriers, because C−O bonds are much stronger than O−O bonds, leading to proposals that step-edge sites are required for CO activation during Fischer−Tropsch synthesis on Co and Ru,[9−11] as also proposed for $N_2$ dissociation during $NH_3$ synthesis on Fe and Ru.[12,13]

Studies on single crystals[14,15] and theoretical treatments[2,9,11,16−18] have suggested that strong bonds cleave on bare surfaces at low-coordination surface atoms. Such atoms, however, may bind adsorbed species strongly and remain inaccessible for direct dissociation steps during catalytic cycles at high coverages often prevalent during catalysis. Such coverages are inaccessible in theoretical studies of flat extended surfaces, but prevail on curved surfaces (where low-index planes are in contact with edge, corner, and defect sites), which allow coverages near saturation, consistent with spectroscopic and kinetic observations.[8,19,20]

Here, we show how diatomic molecules with strong bonds dissociate predominantly via reactions with vicinal co-adsorbed species on crowded low-index surfaces relevant for catalysis, instead of dissociating on vacant terrace or defect sites, which are scarce and less reactive than on bare surfaces. As will be described, H* (from $H_2$) adds to CO* and NO* to weaken their strong bonds by forming *HCOH* and *HNOH*, (*—* indicates binding at two vicinal sites) before C−O or N−O cleavage.[19,21,22] Co-adsorbed $H_2O$ can act as a co-catalyst in forming O−H bonds in *OOH/*HOOH* (from $O_2$) and *HCOH* (from CO) to mediate O−O[23−25] and C−O[20] activations. NO* species disproportionate to form $N_2O$ and O*,[22] and CO* species react with $O_2$* to form $CO_2$ and O* when $H_2$ and $H_2O$ are absent,[8] consistent with the prevalence of bimolecular events even in the absence of a reductant. These bimolecular routes carry an entropic penalty because their transition states are larger and more ordered than those for unimolecular dissociations, but have lower enthalpy barriers, which compensate for unfavorable entropies at the modest temperatures (300−600 K) of these catalytic reactions.

## ■ CO OXIDATION ON Au

Au nanoparticles catalyze the oxidation of CO (to $CO_2$),[26] propene (to propylene oxide),[27] and alkanols (to aldehydes and carboxylic acids) in gaseous[28] or aqueous[23,29] phases at low temperatures (<400 K). The reactivity Au demonstrates contradicts large $O_2$ dissociation barriers on extended Au(111) surfaces (190−215 kJ mol^{−1}).[2,3] Higher turnover rates on smaller Au clusters have suggested that low-coordination sites are necessary for $O_2$ dissociation,[2−4] while higher turnover rates on reducible supports have implicated Au-oxide interfaces.[4−6] Theoretical studies (DFT) have confirmed that low-coordination Au atoms at edges or corners, and at step-edge sites on Au surfaces indeed dissociate $O_2$ with lower barriers than Au(111) surfaces (as low as 90 kJ mol^{−1} on Au(211)),[2] but such barriers remain too large to account for the high CO oxidation reactivity of Au at near-ambient temperatures.[2,26]

Many studies show that water plays a critical role in Au-catalyzed oxidations, even at trace concentrations,[23,30−32] but its mechanistic role remains controversial; it has been variously attributed to promotion of $O_2$ adsorption or dissociation steps, decomposition of unreactive carbonates, assisted reduction of Au cations by CO, and direct reactions of $H_2O$-derived OH* with CO*,[31,32] since OH* species were shown to promote Au-

catalyzed oxidations of CO and alkanols in gaseous ($Au/SiO_2$ doped with NaOH)[33] or alkaline aqueous ($Au/TiO_2$ and Au/C) media.[23,29]

Kinetic and isotopic studies have shed light on the mechanism for $H_2O$-assisted $O_2$ dissociation during CO oxidation on small Au clusters (<5 nm).[25] CO oxidation rates increased with increasing $H_2O$ pressure, and ultimately decreased as $H_2O$* or $H_2O$-derived species (such as OH*) cover Au surfaces at higher pressures (Figure 1). Such
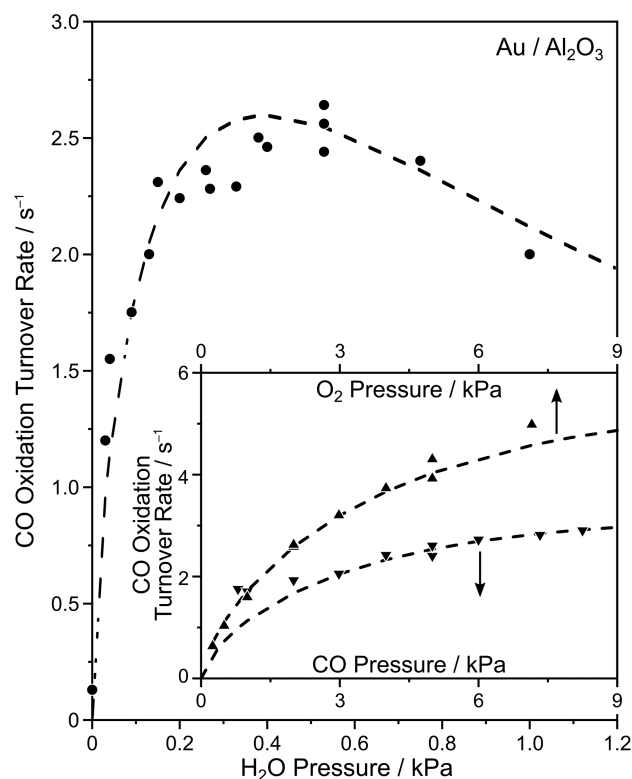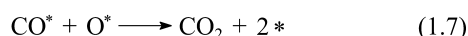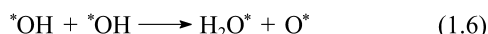


**Figure 1.** Effects of $H_2O$ (●, 5 kPa CO, 2 kPa $O_2$), CO (▼, 2 kPa $O_2$, 0.5 kPa $H_2O$), and $O_2$ (▲, 5 kPa CO, 0.5 kPa $H_2O$) on CO oxidation rates on 0.6 wt % $Au/Al_2O_3$ (3.5 nm Au clusters) at 288 K. Dashed lines represent data fit to eq 3.[21]

enhancements are not caused by water−gas shift reactions, because $CO_2$ did not form from CO−$H_2O$ reactants and $H_2O$ was not consumed during CO−$O_2$ reactions. $CO_2$ formation rates increased with increasing CO and $O_2$ pressure (Figure 1) in a manner consistent with Langmuir−Hinshelwood rate equations on surfaces with CO* and $O_2$* present below saturation coverages.

These data are consistent with kinetically-relevant transition states requiring the concurrent involvement of species derived from CO, $O_2$, and $H_2O$. OOH* species can form via quasi-equilibrated proton transfer from $H_2O$ to $O_2$* (step 1.4 in Scheme 1), and their O−O bond can then cleave by assistance from CO* (step 1.5). OH* species formed (in steps 1.4 and 1.5) then react in a kinetically-irrelevant step to re-form $H_2O$ (step 1.6), which acts as a co-catalyst in this cycle. Scheme 1 leads to a rate equation:

$$r = \frac{\alpha([CO][O_2][H_2O])^{2/3}}{[1 + K_{CO}[CO] + K_{O_2}[O_2] + K_{H_2O}[H_2O]]^2} \quad (3)$$

## Scheme 1. Mechanism for CO Oxidation on Au[a]

$$CO + * \rightleftharpoons CO^* \qquad (1.1)$$

$$O_2 + * \rightleftharpoons O_2^* \qquad (1.2)$$

$$H_2O + * \rightleftharpoons H_2O^* \qquad (1.3)$$

$$O_2^* + H_2O^* \rightleftharpoons {}^*OOH + {}^*OH \qquad (1.4)$$

$${}^*OOH + CO^* \longrightarrow {}^*OH + CO_2 + * \qquad (1.5)$$

$${}^*OH + {}^*OH \longrightarrow H_2O^* + O^* \qquad (1.6)$$

$$CO^* + O^* \longrightarrow CO_2 + 2* \qquad (1.7)$$

[a]The circled double arrow indicates a quasi-equilibrated reaction.

which accurately describes all CO oxidation rate data (288 K, 0.80−8.25 kPa CO, 0.25−7.15 kPa $O_2$, 0.03−1.15 kPa $H_2O$) on Au clusters, irrespective of support ($Al_2O_3$, $TiO_2$, and $Fe_2O_3$);[25] such similar rate equations and mechanistic interpretations for all supports stand in sharp contrast with previous proposals that $O_2$ activation occurs at Au−$TiO_2$[4−6] but not Au−$Al_2O_3$ interfaces. The effects of support on turnover rates under anhydrous conditions (0.54 and 0.08 mol s$^{-1}$ (g-at Au$_{surf}$)$^{-1}$ on $TiO_2$ and $Al_2O_3$, respectively) may reflect instead trace amounts of $H_2O$ adsorbed on such supports, which leaves the reactor with time on stream, leading to the rapid deactivation ubiquitous without added $H_2O$.[31] $H_2O$ (0.5 kPa) increased CO oxidation rates and eliminated support effects on turnover rates (2.55 vs 2.70 mol s$^{-1}$ (g-at Au$_{surf}$)$^{-1}$ on $TiO_2$ vs $Al_2O_3$, respectively). Highly dispersed Au particles have been shown to be necessary for C−H and O−H activations of formic acid (HCOOH). Formic acid decomposition turnover rates (to $H_2$ and $CO_2$ in the absence of $H_2O$) decreased by a factor of ~10 upon treatment of Au/$Al_2O_3$ with 20% $O_2$/He (1000 K for 2 h), which sintered small Au moieties (undetectable by TEM) required for HCOOH decomposition.[34] Similar treatments, however, did not affect CO oxidation turnover rates on Au/$Al_2O_3$, indicating that such small structures are not required for $O_2$ dissociation when $H_2O$ is present.

H-addition to $O_2^*$ before its dissociation was also proposed in Au-catalyzed oxidations of alkanols and polyols.[23] Kinetic and isotopic data, together with DFT calculations, indicated that ethanol and glycerol react with OH groups (present in aqueous media or on Au surfaces) in multiple steps to form acetic and glyceric acids, respectively. C−H and O−H bond activations during oxidative alcohol dehydrogenation proceed via $^*$OH-assisted pathways rather than via reactions with the Au surface,[23] similar to proposals for O$^*$-assisted activations on Au surfaces doped with O$^*$ via $O_3$ decomposition.[35] Alkanol reactions with $^{16}O_2$/$H_2^{18}O$ incorporated only $^{18}O$ within the acids formed at low conversions (reactions with $^{18}O_2$/$H_2^{16}O$ incorporated only $^{16}O$), indicating that OH groups (from $H_2O$) act as the oxidants. $O_2$ reacts with $H_2O$ at Au−solvent interfaces to form $^*$OOH and $^*$HOOH$^*$ species via sequential proton-transfer reactions; the latter species, detected as $H_2O_2$ side products, dissociate to form $^*$OH, thus replacing the OH groups consumed. These cycles at Au−solvent interfaces represent two local electrochemical half-reactions:

$$RCH_2OH + 4OH^- \rightarrow RCOOH + 2H_2O + 4e^- \qquad (4)$$

$$O_2 + 2H_2O + 4e^- \rightarrow 4OH^- \qquad (5)$$
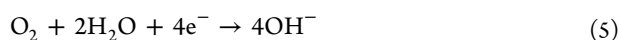
also relevant in direct alkanol fuel cells with Au electrodes.[36]

These studies on Au catalysts show that $H_2O$, added as a co-catalyst, present as a ubiquitous support impurity, formed as an oxidative dehydrogenation product, or used as a solvent, assists $O_2$ activation via proton-transfer reactions that weaken O−O bonds via formation of $^*$OOH and $^*$HOOH$^*$, which undergo subsequent O−O cleavage by reactions with Au surface atoms or adsorbed co-reactants. Such assisted $O_2$ activation routes do not require low-coordination Au atoms or Au−support interfaces, and proceed with low DFT-predicted barriers on Au(111) surfaces,[23] that are inactive for direct $O_2$ dissociation. $H_2O$-assisted $O_2$ activation also exhibits lower barriers than direct $O_2$ dissociation on Pt(111) surfaces at high $H_2O^*$ coverages,[23] mediates electrochemical oxygen reduction at Pt cathodes,[24] and causes $H_2O$ to increase CO oxidation rates on Pt-based catalysts.[25]

## ■ CO OXIDATION ON Pt

Low-temperature (360−473 K) CO oxidation on Pt occurs on surfaces saturated with CO$^*$,[8,37−39] as with CO hydrogenation (Fischer−Tropsch synthesis) on Ru and Co catalysts.[19,40] CO oxidation rates are proportional to $O_2$ pressure and inversely dependent on CO pressure on Pt[8,37] (Figure 2), Pd,[39] and Rh[38] catalysts:

$$r = \frac{\alpha[O_2]}{[1 + K_{CO}[CO]]} \qquad (6)$$

The first-order dependence on $O_2$ pressure may reflect irreversible molecular $O_2$ adsorption as the sole kinetically-relevant step (step 2A.2 in Scheme 2),[37] which requires that
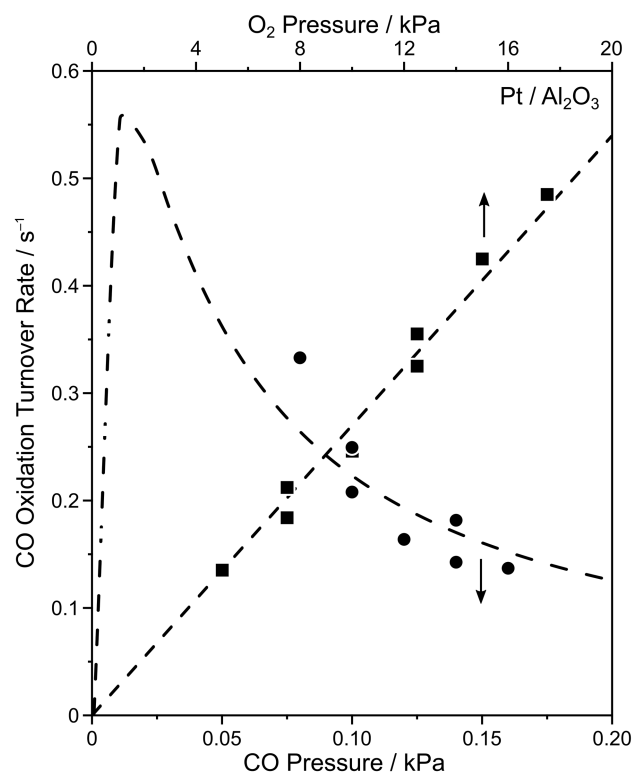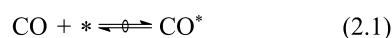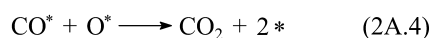


**Figure 2.** Effects of CO (●, 10 kPa $O_2$) and $O_2$ (■, 0.1 kPa CO) on CO oxidation rates on 2.0 wt % Pt/$Al_2O_3$ (11 nm Pt clusters) at 443 K. Dashed lines represent data fit to eq 6.[8]
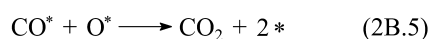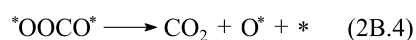
**Scheme 2. Mechanisms for Low-Temperature CO Oxidation on Pt-Group Metals**

$$CO + * \rightleftharpoons CO^* \qquad (2.1)$$

*Irreversible $O_2$ adsorption and direct $O_2^*$ dissociation*

$$O_2 + * \longrightarrow O_2^* \qquad (2A.2)$$

$$O_2^* + * \longrightarrow 2\,O^* \qquad (2A.3)$$

$$CO^* + O^* \longrightarrow CO_2 + 2* \qquad (2A.4)$$

*Reversible $O_2$ adsorption and $CO^*$-assisted $O_2^*$ dissociation*

$$O_2 + * \rightleftharpoons O_2^* \qquad (2B.2)$$

$$O_2^* + CO^* \longrightarrow {}^*OOCO^* \qquad (2B.3)$$

$$^*OOCO^* \longrightarrow CO_2 + O^* + * \qquad (2B.4)$$

$$CO^* + O^* \longrightarrow CO_2 + 2* \qquad (2B.5)$$

$O_2^*$ dissociation occurs with smaller barriers than $O_2^*$ desorption, consistent with theoretical treatments on bare Pt(111) surfaces.[7] At 0.44 ML CO* coverage, however, $O_2^*$ desorption barriers are 33 kJ mol$^{-1}$ smaller than those for $O_2^*$ dissociation,[7] indicating that molecular $O_2$ adsorption would be quasi-equilibrated during steady-state catalysis at relevant CO* coverages. Quasi-equilibrated adsorption (step 2A.2) and subsequent $O_2^*$ dissociation on vicinal vacancies (*) (step 2A.3) would give rates proportional to $[CO]^{-2}$ on CO*-saturated surfaces, while quasi-equilibrated dissociation (step 2A.3) and subsequent irreversible reactions of O* with CO* (step 2A.4) would give rates proportional to $[O_2]^{0.5}$. These two routes have been proposed previously but are inconsistent with rate data.[37−39]

DFT treatments at CO* coverages near 1 ML require nanoparticle models (cuboctahedral Pt$_{201}$ consisting of 201 atoms; ∼1.5 nm diameter) because flat extended surfaces cannot sufficiently relax CO* adlayers.[8] On Pt$_{201}$ clusters with 1 ML CO*, $O_2^*$ adsorption requires vacancy formation events (CO* desorption) that are endothermic (79 kJ mol$^{-1}$). $O_2^*$ species react with vicinal CO* to form *OOCO* species (step 2B.3 in Scheme 2) with small barriers (15 kJ mol$^{-1}$). The subsequent dissociation of *OOCO* into $CO_2$ and O* (step 2B.4) is essentially barrierless (2 kJ mol$^{-1}$), indicating that *OOCO* formation is irreversible and that bimolecular $O_2$ dissociation routes prevail over direct $O_2$ dissociation events that require additional energetically disfavored CO* desorption events. Unlike $O_2$ dissociation on Au, $O_2$ can dissociate via direct interactions with Pt atoms on low-index bare surfaces, but such surfaces become covered with CO* during steady-state catalysis, rendering them much less reactive than bare Pt surfaces. CO* also binds strongly to Rh and Pd surfaces, which exhibit identical CO oxidation rate equations (eq 6),[38,39] suggesting that $O_2$ dissociation occurs via bimolecular mechanisms similar to Scheme 2B on Rh and Pd catalysts.

## ■ NO REDUCTION BY $H_2$ ON Pt

Nitric oxide (NO) (BDE of 631 kJ mol$^{-1}$) has a significantly stronger bond than $O_2$ (BDE of 498 kJ mol$^{-1}$).[1] As a result, NO dissociation barriers (236 kJ mol$^{-1}$)[22] are much higher than those for $O_2$ (31 kJ mol$^{-1}$)[7] on bare Pt(111) surfaces.

NO−$H_2$ reactions occur at modest temperatures (<500 K), thus making $H_2$ an attractive reductant. Previous studies of $H_2$, $H_2O$, and $O_2$ effects on NO−$H_2$ rates and selectivities for Pt,[41] Pd,[42] and Rh[43] catalysts have reached contradictory conclusions about the mechanism for NO activation. Large NO* dissociation activation barriers (236 kJ mol$^{-1}$) have led to proposals that NO* activation must require step-edge defect sites on Pt[18] and Ru,[17] based on theoretical assessments on extended bare surfaces.

NO−$H_2$ turnover rates are proportional to $H_2$ pressure at low pressures (<5 kPa $H_2$) and become independent of $H_2$ pressure at higher pressures (>500 kPa) (Figure 3),[22]
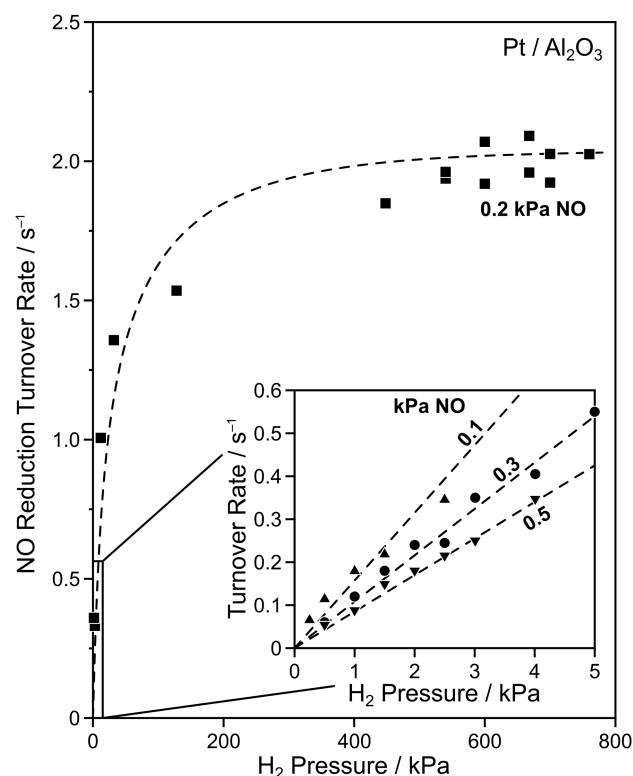


**Figure 3.** Effects of $H_2$ on NO−$H_2$ turnover rates from 1 to 760 kPa $H_2$ at 0.2 kPa NO (■, 398 K) and at <5 kPa $H_2$ (inset, 383 K) at 0.1 kPa NO (▲), 0.3 kPa NO (●), and 0.5 kPa NO (▼) on 0.6 wt % Pt/Al$_2$O$_3$ (4.4 nm Pt clusters).[22]

consistent with NO activation via Scheme 3D on surfaces saturated with NO* and H* species (and few vacant sites), leading to rates,

$$r = \frac{\alpha[NO][H_2]}{\left[K_{H_2}^{1/2}[H_2]^{1/2} + K_{NO}[NO]\right]^2} \qquad (7)$$
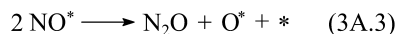
consistent with those measured (1−760 kPa $H_2$, 0.05−0.70 kPa NO; 383−453 K) on Al$_2$O$_3$-supported Pt clusters (1.7, 4.4, and 13.7 nm mean diameter).[22] Turnover rates depend weakly on Pt cluster size, inconsistent with requirements for defect sites in kinetically-relevant NO* activation steps.[18] DFT-derived enthalpies and free energies on Pt(111) surfaces with 0 to 5/9 ML coverages of spectator NO* species indicate that NO*-assisted (step 3A.3 in Scheme 3) and direct (step 3B.3) NO* activation steps would be irreversible and thus kinetically-relevant, making these two routes inconsistent with rate data

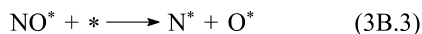**Scheme 3. NO Activation Mechanisms during NO−H$_2$ Reactions**
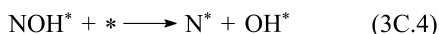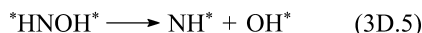
*Quasi-equilibrated reactant adsorption*

$$NO + * \rightleftharpoons NO^* \qquad (3.1)$$

$$H_2 + 2* \rightleftharpoons 2 H^* \qquad (3.2)$$

*NO\*-assisted NO\* activation*

$$2 NO^* \longrightarrow N_2O + O^* + * \qquad (3A.3)$$

*Direct NO\* dissociation*

$$NO^* + * \longrightarrow N^* + O^* \qquad (3B.3)$$

*H\*-assisted NO\* activation (via NOH\*)*

$$NO^* + H^* \rightleftharpoons NOH^* \qquad (3C.3)$$

$$NOH^* + * \longrightarrow N^* + OH^* \qquad (3C.4)$$

*H\*-assisted NO\* activation (via \*HNOH\*)*

$$NO^* + H^* \rightleftharpoons HNO^* \qquad (3D.3)$$

$$HNO^* + H^* \longrightarrow {}^*HNOH^* \qquad (3D.4)$$

$${}^*HNOH^* \longrightarrow NH^* + OH^* \qquad (3D.5)$$

described by eq 7.[18] H\*-assisted NO\* activation via NOH\* intermediates (Scheme 3C) is mediated by a transition state with only one H atom, leading to a $[H_2]^{0.5}$ numerator term of the rate law that is inconsistent with eq 7. H\*-assisted NO\* activation via sequential H-additions to form \*HNOH\* species (Scheme 3D) is consistent with rate data (eq 7), and exhibits the lowest enthalpy and free energy barriers (relative to an NO\*-covered surface) among the four routes in Scheme 3 at all NO\* coverages (Figure 4). These data and theoretical treatments indicate that bimolecular NO activation routes
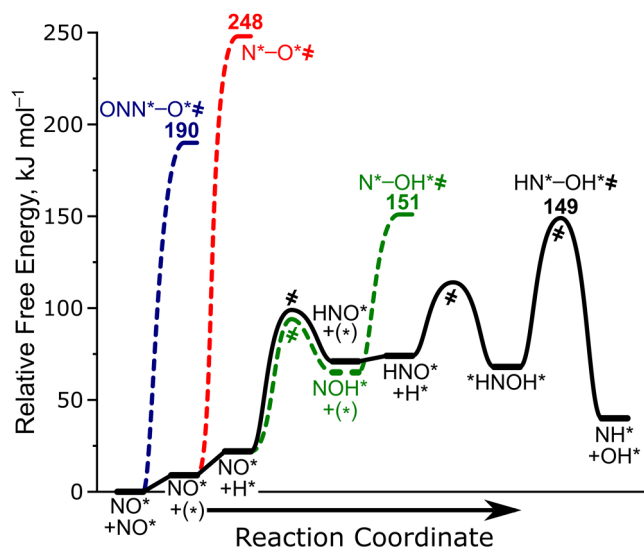
prevail over direct routes at all coverages, in contrast with O$_2$ dissociation during CO oxidation on Pt, which occurs via bimolecular routes only at high CO\* coverages because of a dearth of vacant sites. Such differences reflect the much stronger bonds in NO (than O$_2$), which render even bare Pt(111) surfaces less reactive for direct dissociation than for H\*-assisted dissociation routes that weaken N−O bonds by H atoms. In the absence of H$_2$, such as during NO reduction with CO, NO\*-assisted NO\* activation reactions prevail over direct NO\* dissociations, and reactions of NO\* with CO\* (similar to O$_2$\*−CO\* reactions in Scheme 2B) may become relevant.

## ■ FISCHER−TROPSCH SYNTHESIS ON Co AND Ru CATALYSTS

Fischer−Tropsch synthesis (FTS) produces liquid fuels from synthesis gas (CO + H$_2$) derived from natural gas, coal, or biomass.[40] The pathways by which C−O bonds cleave have remained controversial.[10,11,14,15,21,40,44] C−O bonds in CO\* can dissociate directly to form C\* and O\* via reactions with vicinal vacant sites (\*), which are present as minority species on the CO\*-saturated surfaces prevalent in practice. CO\* can also react with H\* to weaken its C−O bond before cleavage in H\*-assisted CO activation mechanisms. FTS occurs on Co and Ru surfaces nearly saturated with CO\*, as shown from measured rates that depend inversely on CO pressure (Figure 5) and infrared spectra during FTS.[19,21,40,45−47] FTS rates are proportional to H$_2$ pressure on Co and Ru catalysts at all relevant FTS reaction conditions (453−520 K; Figure 5). The accepted rate equation for this reaction (eq 8)[19,21,40,45,46] is



**Figure 4.** DFT-calculated free energy diagram (at 423 K) for NO\* activation via NO\*-assisted (blue, dashed), direct dissociation (red, dashed), H\*-assisted via NOH\* (green, dashed), and H\*-assisted via \*HNOH\* (black) routes at 3/9 ML spectator NO\* on Pt(111) surfaces. Effective free energy barriers represent the energy required to form transition states from an NO\*-covered Pt surface.[18]
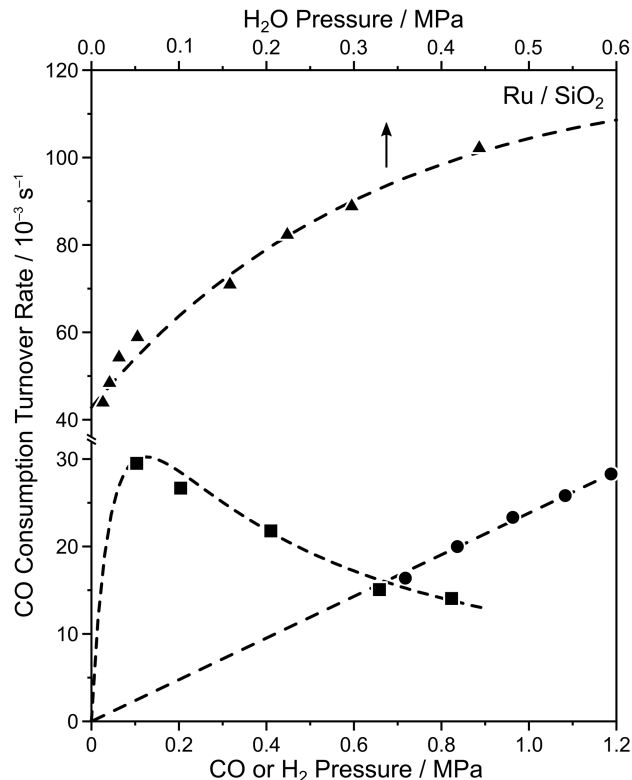


**Figure 5.** Effects of CO (■, 1.1 MPa H$_2$, 0.01 MPa H$_2$O), H$_2$ (●, 0.65 MPa CO, 0.02 MPa H$_2$O), and H$_2$O (▲, 0.5 MPa CO, 2.2 MPa H$_2$) on FTS rates on 5 wt % Ru/SiO$_2$ (7 nm Ru clusters) at 518 K. Dashed lines represent data fit to eq 8.[25]

consistent with a kinetically-relevant transition state involving two H atoms and one CO-derived moiety, making it consistent with H*-assisted dissociation (via *HCOH* species) instead of direct CO* dissociation.

$$r = \frac{\alpha[\text{CO}][\text{H}_2]}{[1 + K_{\text{CO}}[\text{CO}]]^2} \qquad (8)$$
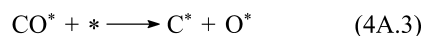
Large barriers for direct CO* dissociation (step 4A.3 in Scheme 4) on Co(0001) (230 kJ mol$^{-1}$)[9] and Ru(0001) (227

**Scheme 4. CO Activation Mechanisms during Fischer–Tropsch Synthesis on Ru and Co Catalyst**
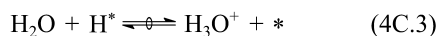
*Quasi-equilibrated reactant adsorption*

$$\text{CO} + * \rightleftharpoons \text{CO}^* \qquad (4.1)$$

$$\text{H}_2 + 2* \rightleftharpoons 2\,\text{H}^* \qquad (4.2)$$

*Direct CO* dissociation*

$$\text{CO}^* + * \longrightarrow \text{C}^* + \text{O}^* \qquad (4A.3)$$

*H*-assisted CO* activation*

$$\text{CO}^* + \text{H}^* \rightleftharpoons \text{HCO}^* \qquad (4B.3)$$

$$\text{HCO}^* + \text{H}^* \longrightarrow \text{CH}^* + \text{OH}^* \qquad (4B.4)$$

*H$_2$O and H*-assisted CO* activation*

$$\text{H}_2\text{O} + \text{H}^* \rightleftharpoons \text{H}_3\text{O}^+ + * \qquad (4C.3)$$

$$\text{CO}^* + \text{H}_3\text{O}^+ \rightleftharpoons \text{COH}^* + \text{H}_2\text{O} \qquad (4C.4)$$

$$\text{COH}^* + \text{H}^* \xrightarrow{\text{H}_2\text{O}} \text{CH}^* + \text{OH}^* \qquad (4C.5)$$

kJ mol$^{-1}$)[10] are consistent with large BDE values for CO (1070 kJ mol$^{-1}$)[1], and have led to proposals that direct CO* dissociation requires low-coordination surface sites (e.g., steps or edges). These conclusions are consistent with CO* dissociation rates at 450−500 K on atomically stepped Ru(109) surfaces, which were suppressed by blocking step-sites with C atoms.[14] Indeed, DFT-derived direct CO* dissociation barriers on bare stepped surfaces of Co[9,11] (68−136 kJ mol$^{-1}$) and Ru[10,11] (47−89 kJ mol$^{-1}$) are much smaller than on Co(0001) and Ru(0001) surfaces. FTS, however, occurs on curved surfaces crowded with CO* on which a dearth of vacant sites and the strong binding of CO* at low-coordination sites render such sites unavailable for FTS turnovers. Furthermore, turnover rates on Co[40,44] and Ru[48] catalysts increase with increasing particle size, and become constant for particles larger than 6−10 nm, indicating that turnovers predominantly occur on low-index terrace sites prevalent on larger clusters. H*-assisted CO* activation fully reconciles (1) rates that are proportional to H$_2$ pressure, (2) particle size effects that show that CO* activates on low-index terrace sites, and (3) DFT treatments indicating that CO* cannot activate directly on such low-index Co and Ru surfaces, but can do so on such surfaces via H*-assistance.

The evidence for defect-catalyzed CO* dissociation during FTS turnovers[9−11,14,15] was obtained from theory and experiments on essentially bare surfaces, instead of surfaces that are nearly saturated with CO* present at practical FTS conditions.[19,21,40,45−47] Recent theoretical studies of CO* activation on sites with varying coordination on curved surfaces at catalytically relevant CO* coverages[19,20] have resolved these

enduring contradictions by demonstrating that H*-assisted CO* activation is preferred over direct CO* dissociation at all sites, irrespective of their metal-atom coordination.[19,20] These studies used the curved surfaces of small cuboctahedral Ru particles (∼200 atoms, ∼1.7 nm, shown in Figure 6), which
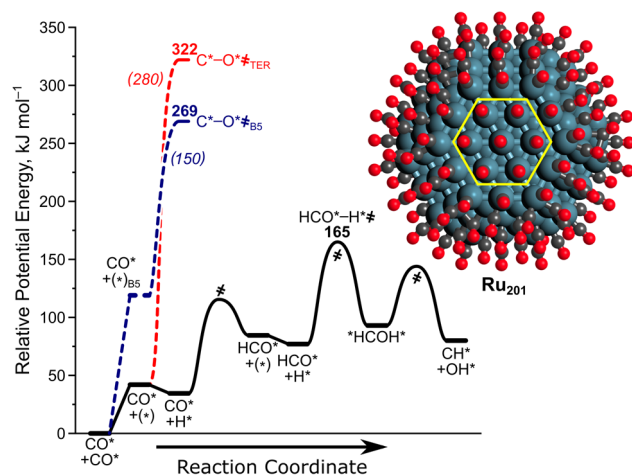


**Figure 6.** DFT-derived potential energy diagram for CO* activation via direct dissociation on step-edge (B$_5$) sites (blue, dashed lines) and terrace sites (red, dashed lines) and via H*-assisted CO* activation (black lines) on terrace sites. Effective activation barriers (bold print) represent the energy to form the transition state from a CO*-covered surface. The Ru$_{201}$ model (inset) used to model reactions on the terrace sites (outlined in yellow) is also shown.[19]

allow exothermic CO* adsorption (−108 kJ mol$^{-1}$) even at 1 ML coverages, in contrast with the endothermic adsorption prevalent on flat extended Ru(0001) surfaces (+18 kJ mol$^{-1}$).[19,20] The very different adsorption energies of CO* on Ru$_{201}$ particles and Ru(0001) extended surfaces at 1 ML CO* are not reflected in their respective bare surfaces, on which CO* binds with similar strength (Ru(0001), −160 kJ mol$^{-1}$; Ru$_{201}$, −159 kJ mol$^{-1}$).[19] High CO* coverages cause longer Ru−Ru bonds and lateral CO* adlayer relaxation on Ru$_{201}$ particles; these are absent in periodic Ru(0001) surfaces due to the periodic nature of these calculations.

The Ru particles in these recent studies expose low-index terrace sites, step-edge (B$_5$) sites, and corner sites, thus allowing a rigorous theoretical assessment of coordination effects on C−O bond cleavage via direct and H-assisted routes.[19] Intrinsic barriers for direct CO* activation on step-edge sites are much larger at 1.07 ML CO* on Ru$_{201}$ (150 kJ mol$^{-1}$) than at 0.25 ML CO* on Ru(10$\bar{1}$5) surfaces (89 kJ mol$^{-1}$)[10] because of repulsion among co-adsorbed CO*. Effective activation barriers (which include the CO* desorption energy to form the required vacancy) for direct CO* dissociation on step-edge sites (269 kJ mol$^{-1}$) are smaller than on low-index Ru(111) terraces (322 kJ mol$^{-1}$; Figure 6), but remain much larger than measured activation energies (∼120 kJ mol$^{-1}$)[19] and those for H-assisted CO* activation.

In H*-assisted CO dissociation routes on low-index planes of Ru$_{201}$ particles, the first H-addition forms HCO* (step 4B.3) in a quasi-equilibrated step; the second H* addition is irreversible and forms *HCOH* (Figure 6), whose C−O bond then cleaves to form CH* and OH* (step 4B.4).[19] CO* activation thus proceeds via H*-assisted routes involving *HCOH* formation and dissociation.[21] These H*-assisted routes lead to

the rate equation (eq 8) that describes most reported FTS rate data on Co and Ru catalysts at conditions relevant to their practice.[19,21,40,45,46] The effective activation barrier for H*-assisted CO activation is 165 kJ mol$^{-1}$, a value 104−191 kJ mol$^{-1}$ smaller than that for direct CO* dissociation on terrace (322 kJ mol$^{-1}$), corner (356 kJ mol$^{-1}$), or step-edge (269 kJ mol$^{-1}$) sites (Figure 6).[19] These DFT-derived barriers show that CO* species react with H* on crowded low-index Ru surfaces to form *HCOH* species before C−O activation, instead of reacting with vacant sites present as minority species during FTS catalysis. Parallel calculations performed on Co(0001) surfaces at 0.5 ML CO* are also consistent with CO* activation via *HCOH* intermediates.[21] These H*-assisted CO activation routes are analogous to the H*-assisted NO activation routes via *HNOH* intermediates described earlier in this Account.

O atoms in CO are predominantly removed as H$_2$O during FTS on Co and Ru catalysts.[19,21,40] H$_2$O increases FTS rates on Co[40,47,49] and Ru[20] catalysts (Figure 5) but at high pressures decreases rates because of competitive adsorption of H$_2$O-derived species and CO-derived reactive intermediates. H$_2$O decreases activation barriers from 152 to 75 kJ mol$^{-1}$ for H-addition to CO* to form COH* (steps 4C.3 and 4C.4),[20] which allows COH* formation steps, otherwise kinetically inaccessible, to become quasi-equilibrated. These COH* species H-bond with H$_2$O and react with another H* to form *HCOH*, which cleaves its C−O bond (to form CH* and OH*) in the kinetically-relevant step (step 4C.5). The effective enthalpy barrier (which includes energies for all steps forming the kinetically-relevant transition state from a CO*-covered surface) for the H$_2$O-mediated route is 129 kJ mol$^{-1}$, which is 64 kJ mol$^{-1}$ lower than for the "anhydrous" H*-assisted route. This enthalpic stabilization is partially offset by entropy losses caused by H$_2$O binding at H$_2$O-mediated transition states that lead to H$_2$O-assisted DFT-derived free energy barriers 5 kJ mol$^{-1}$ larger than for anhydrous routes rather than the 8 kJ mol$^{-1}$ lower values that were experimentally measured, but consistent with their parallel contributions to CO activation pathways.[20] Such H$_2$O effects on O−H formation rates were described above for O$_2$ activation in Au-catalyzed oxidations. H$_2$O-mediated H*-assisted CO dissociation provides another example of how co-adsorbed species weaken (via reduction) and assist the cleavage of strong molecular bonds. These routes become most influential at the high coverages prevalent during catalysis, because surfaces contain few, weakly-binding exposed atoms, and defect sites stabilize unreactive species.

## AMMONIA SYNTHESIS ON Fe AND Ru

N$_2$ dissociation during NH$_3$ synthesis on Ru and Fe was one of the first reactions proposed to take place on defect sites.[12,13] Biological N$_2$ fixation in nitrogenases, in contrast, occurs at near-ambient temperatures via sequential addition of H$^+$/e$^-$ pairs (from MgATP hydrolysis) to N$_2$ to form bound NH$_2$NH$_2$ species before N−N cleavage.[50]

DFT-derived free energy barriers for direct and H*-assisted (via NNH* formation and dissociation) N−N cleavage on bare Ru(0001) surfaces were similar (247 kJ mol$^{-1}$) at 673 K.[51] These values give a ratio of direct to H*-assisted activation rates,

$$\frac{r_{\text{direct}}}{r_{\text{H-assist}}} = e^{((\Delta G^{\ddagger}_{\text{H-assist}} - \Delta G^{\ddagger}_{\text{direct}})/(RT))}(\text{H}_2/\text{bar})^{-0.5}$$

(9)

that is smaller than one at high-pressure NH$_3$ synthesis conditions (600−773 K, >5 bar H$_2$), Figure 7. H*-assisted N$_2$
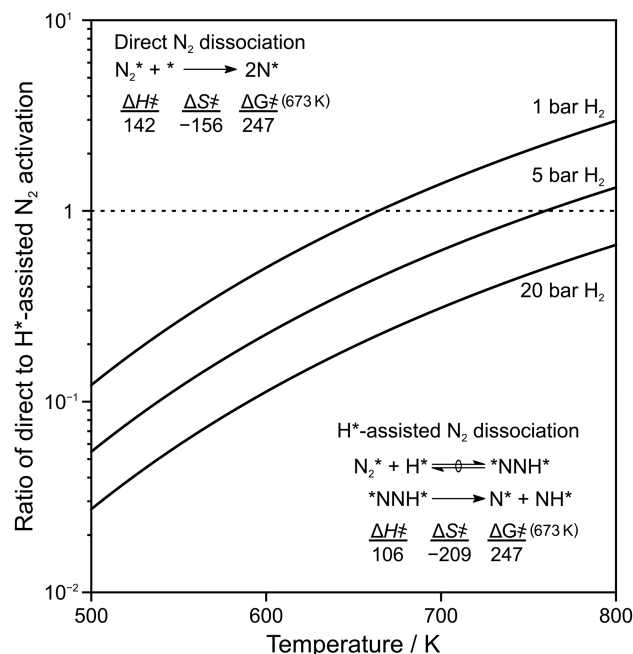


**Figure 7.** DFT-calculated ratio of direct to H*-assisted N$_2$ activation at various H$_2$ pressures and temperatures on Ru(0001) surfaces along with the enthalpy, entropy, and free energy barriers for each mechanism with respect to a bare Ru surface.

cleavage that occurs through transition states with more H atoms (N$_2$H$_2$*) shows larger effective free energy barriers (≥286 kJ mol$^{-1}$) than direct or H*-assisted N$_2$ activation via NNH*, ruling out such routes. Thus, on Ru(0001) surfaces, H*-assisted N$_2$ activation (via NNH*) prevails over direct dissociation; however, its barrier (247 kJ mol$^{-1}$) is higher than expected from measured turnover rates; thus, step-edge sites may be required for N$_2$ activation at the temperatures of NH$_3$ synthesis practice.[13] Further investigation is required to determine the kinetic effects of H$_2$ pressure and relevant coverages of abundant surface intermediates, such as NH$_x$* ($x$ = [0, 3]) species.

## OUTLOOK

Experimental and theoretical inquiries into the reactivity of bare extended surfaces tend to magnify the significance of defect sites in activations of strong chemical bonds. In doing so, a seemingly consistent picture of reactivity obscures what matters most at high coverages often present at practical conditions of catalysis. Theoretical treatments, when brought to these relevant coverages through the use of curved surfaces, show how low-index planes are able to activate strong bonds through bimolecular events involving co-adsorbed intermediates. The methods to address crowded and curved surfaces, in theory and experiment, are available. DFT calculations can examine surfaces of metal particles (∼500 atoms), which contain exposed atoms with different coordination. The relaxation of intermolecular repulsion on such curved surfaces allows monolayer coverages, while dispersive forces, now incorporated into many functionals, account for the van der Waals forces that strongly influence the stability of adsorbed intermediates and

transition states at high coverages. Rate, isotopic, and spectroscopic data at conditions of strict kinetic control have sharpened our proposals about the relevant intermediates and their reaction paths. Today, experiment and theory are closer than ever before to being able to probe the same chemical event at the level of surface-catalyzed elementary steps occurring within the local environments that prevail during the practice of relevant catalysis. After more than a century of inquiry into the mechanistic details of heterogeneous catalysis, we find surprises, brought to light by the emerging clarity of our inquiries.

## ■ SUMMARY

High coverages, often present in catalytic practice, result in few vacancies at defect sites, which are made more inert through co-adsorbate interactions but are catalytically significant on bare surfaces for direct activations of strongly bound diatomic species ($O_2$, NO, and CO). Low-index surfaces, inactive for direct dissociation, instead catalyze bimolecular reactions between co-adsorbed reagents and these species. H-addition reactions (from $H_2$ or $H_2O$) act to reduce the double or triple bonds present in $O_2$, NO, and CO to *HOOH*, *HNOH*, and *HCOH* intermediates prior to bond cleavage. Similarly, direct reactions of $O_2$*−CO*, NO*−NO*, and NO*−CO* result in O−O or N−O cleavages without H-involvement or direct dissociation across vacancies. These bimolecular routes are entropically disfavored compared to direct dissociation because of the involvement of multiple reagents within their transition states, but such penalties are compensated by lower activation enthalpies that govern rates at the modest temperatures (300−600 K) common in the reactions described in this Account.

## ■ AUTHOR INFORMATION

### Notes

The authors declare no competing financial interest.

### Biographies

**David Hibbitts** is currently a postdoctoral fellow at the University of California, Berkeley. He received his B.S. in Chemical Engineering from Clemson University in 2007 and his Ph.D. in Chemical Engineering from the University of Virginia in 2012. His Ph.D. research included theoretical investigations of aqueous phase oxidation and hydrogenolysis reactions on metal catalysts with Professor Matthew Neurock.

**Enrique Iglesia** is the Theodore Vermeulen Chair in Chemical Engineering at the University of California, Berkeley, and a Faculty Senior Scientist at the E. O. Lawrence Berkeley National Laboratory. He received his Ph.D. in Chemical Engineering in 1982 from Stanford University. In 1993, he joined the Berkeley faculty after 11 years at Exxon Research and Engineering. He acts as Director of the Berkeley Catalysis Center, President of the North American Catalysis Society, and is the former Editor-in-Chief of *Journal of Catalysis*.

## ■ ACKNOWLEDGMENTS

## ■ REFERENCES

(1) BDE (kJ mol$^{-1}$) of $O_2$ (498), NO (631), $N_2$ (946), and CO (1075) from DarWent, B. *Bond Dissociation Energies in Simple Molecules*; National Bureau of Standards: Washington, DC, 1970.

(2) Liu, Z.-P.; Hu, P.; Alavi, A. Catalytic Role of Gold in Gold-Based Catalysts: A Density Functional Theory Study on the CO Oxidation on Gold. *J. Am. Chem. Soc.* **2002**, *124*, 14770−14779.

(3) Bond, G.; Louis, C.; Thompson, D. T. *Catalysis by Gold*; Imperial College Press: London, 2006.

(4) Boccuzzi, F.; Chiorino, A.; Manzoli, M.; Lu, P.; Akita, T.; Ichikawa, S.; Haruta, M. Au/$TiO_2$ Nanosized Samples: A Catalytic, TEM, and FTIR Study of the Effect of Calcination Temperature on the CO Oxidation. *J. Catal.* **2001**, *202*, 256−267.

(5) Green, I.; Tang, W.; Neurock, M.; Yates, J. Spectroscopic Observation of Dual Catalytic Sites during Oxidation of CO on a Au/$TiO_2$ Catalyst. *Science* **2011**, *333*, 736−739.

(6) Janssens, T.; Clausen, B.; Hvolbæk, B.; Falsig, H.; Christensen, C.; Bligaard, T.; Nørskov, J. Insights into the Reactivity of Supported Au Nanoparticles: Combining Theory and Experiments. *Top. Catal.* **2007**, *44*, 15−26.

(7) Shan, B.; Kapur, N.; Hyun, J.; Wang, L.; Nicholas, J.; Cho, K. CO-Coverage-Dependent Oxygen Dissociation on Pt(111) Surface. *J. Phys. Chem. C* **2009**, *113*, 710−715.

(8) Allian, A.; Takanabe, K.; Fujdala, K.; Hao, X.; Truex, T.; Cai, J.; Buda, C.; Neurock, M.; Iglesia, E. Chemisorption of CO and Mechanism of CO Oxidation on Supported Platinum Nanoclusters. *J. Am. Chem. Soc.* **2011**, *133*, 4498−4517.

(9) Ge, Q.; Neurock, M. Adsorption and Activation of CO over Flat and Stepped Co Surfaces: A First Principles Analysis. *J. Phys. Chem. B* **2006**, *110*, 15368−15380.

(10) Ciobica, I.; van Santen, R. Carbon Monoxide Dissociation on Planar and Stepped Ru(0001) Surfaces. *J. Phys. Chem. B* **2003**, *107*, 3808−3812.

(11) Shetty, S.; van Santen, R. Hydrogen Induced CO Activation on Open Ru and Co Surfaces. *Phys. Chem. Chem. Phys.* **2010**, *12*, 6330−6332.

(12) Ozaki, A.; Taylor, H. Kinetics and Mechanism of the Ammonia Synthesis. *Proc. R. Soc. London, Ser. A* **1960**, *258*, 47−62.

(13) Dahl, S.; Logadottir, A.; Egeberg, R.; Larsen, J.; Chorkendorff, I.; Tornqvist, E.; Norskov, J. Role of Steps in $N_2$ Activation on Ru(0001). *Phys. Rev. Lett.* **1999**, *83*, 1814−1817.

(14) Zubkov, T.; Morgan, G.; Yates, J.; Kühlert, O.; Lisowski, M.; Schillinger, R.; Fick, D.; Jänsch, H. The Effect of Atomic Steps on Adsorption and Desorption of CO on Ru(109). *Surf. Sci.* **2003**, *526*, 57−71.

(15) Tison, Y.; Nielsen, K.; Mowbray, D.; Bech, L.; Holse, C.; Calle-Vallejo, F.; Andersen, K.; Mortensen, J.; Jacobsen, K.; Nielsen, J. Scanning Tunneling Microscopy Evidence for the Dissociation of Carbon Monoxide on Ruthenium Steps. *J. Phys. Chem. C* **2012**, *116*, 14350−14359.

(16) Shetty, S.; Jansen, A.; van Santen, R. CO Dissociation on the Ru(11$\bar{2}$1) Surface. *J. Phys. Chem. C* **2008**, *112*, 14027−14033.

(17) Hammer, B. Bond Activation at Monatomic Steps: NO Dissociation at Corrugated Ru(0001). *Phys. Rev. Lett.* **1999**, *83*, 3681−3684.

(18) Backus, E.; Eichler, A.; Grecea, M.; Kleyn, A.; Bonn, M. Adsorption and Dissociation of NO on Stepped Pt (533). *J. Chem. Phys.* **2004**, *121*, 7946−7954.

(19) Loveless, B.; Buda, C.; Neurock, M.; Iglesia, E. CO Chemisorption and Dissociation at High Coverages during CO Hydrogenation on Ru Catalysts. *J. Am. Chem. Soc.* **2013**, *135*, 6107−6121.

(20) Hibbitts, D.; Loveless, B.; Neurock, M.; Iglesia, E. Mechanistic Role of Water on the Rate and Selectivity of Fischer−Tropsch Synthesis on Ruthenium Catalysts. *Angew. Chem., Int. Ed.* **2013**, *52*, 12273−12278.

(21) Ojeda, M.; Nabar, R.; Nilekar, A.; Ishikawa, A.; Mavrikakis, M.; Iglesia, E. CO Activation Pathways and the Mechanism of Fischer−Tropsch Synthesis. *J. Catal.* **2010**, *272*, 287−297.

(22) Hibbitts, D.; Jiménez, R.; Yoshimura, M.; Weiss, B.; Iglesia, E. Catalytic NO Activation and NO-$H_2$ Reaction Pathways. *J. Catal.* **2014**, *319*, 95−109.

(23) Zope, B.; Hibbitts, D.; Neurock, M.; Davis, R. Reactivity of the Gold/Water Interface during Selective Oxidation Catalysis. *Science* **2010**, *330*, 74−78.

(24) Janik, M.; Taylor, C.; Neurock, M. First-Principles Analysis of the Initial Electroreduction Steps of Oxygen over Pt(111). *J. Electrochem. Soc.* **2009**, *156*, B126−B135.

(25) Ojeda, M.; Zhan, B.; Iglesia, E. Mechanistic Interpretation of CO Oxidation Turnover Rates on Supported Au Clusters. *J. Catal.* **2012**, *285*, 92−102.

(26) Haruta, M.; Yamada, N.; Iijima, S.; Kobayashi, T. Gold Catalysts Prepared by Coprecipitation for Low-Temperature Oxidation of Hydrogen and of Carbon Monoxide. *J. Catal.* **1989**, *115*, 301−309.

(27) Ojeda, M.; Iglesia, E. Catalytic Epoxidation of Propene with $H_2O$-$O_2$ Reactants on Au/$TiO_2$. *Chem. Commun.* **2009**, *2*, 352−354.

(28) Enache, D.; Knight, D.; Hutchings, G. Solvent-Free Oxidation of Primary Alcohols to Aldehydes Using Supported Gold Catalysts. *Catal. Lett.* **2005**, *103*, 43−52.

(29) Ketchie, W.; Murayama, M.; Davis, R. Promotional Effect of Hydroxyl on the Aqueous Phase Oxidation of Carbon Monoxide and Glycerol over Supported Au Catalysts. *Top. Catal.* **2007**, *44*, 307−317.

(30) Daté, M.; Okumura, M.; Tsubota, S.; Haruta, M. Vital Role of Moisture in the Catalytic Activity of Supported Gold Nanoparticles. *Angew. Chem., Int. Ed.* **2004**, *43*, 2129−2132.

(31) Kung, H.; Kung, M.; Costello, C. Supported Au Catalysts for Low Temperature CO Oxidation. *J. Catal.* **2003**, *216*, 425−432.

(32) Braunchweig, B.; Hibbitts, D.; Neurock, M.; Wieckowski, A. Electrocatalysis: A Direct Alcohol Fuel Cell and Surface Science Perspective. *Catal. Today* **2013**, *202*, 197−209.

(33) Qian, K.; Zhang, W.; Sun, H.; Fang, J.; He, B.; Ma, Y.; Jiang, Z.; Wei, S.; Yang, J.; Huang, W. Hydroxyls-Induced Oxygen Activation on "Inert" Au Nanoparticles for Low-Temperature CO Oxidation. *J. Catal.* **2011**, *277*, 95−103.

(34) Ojeda, M.; Iglesia, E. Formic Acid Dehydrogenation on Au-Based Catalysts at near-Ambient Temperatures. *Angew. Chem., Int. Ed.* **2009**, *48*, 4800−4803.

(35) Madix, R.; Friend, C.; Liu, X. Anticipating Catalytic Oxidation Reactions on Gold at High Pressure (Including Liquid Phase) from Ultrahigh Vacuum Studies. *J. Catal.* **2008**, *258*, 410−413.

(36) Kwon, Y.; Lai, S.; Rodriguez, P.; Koper, M. Electrocatalytic Oxidation of Alcohols on Gold in Alkaline Media: Base or Gold Catalysis? *J. Am. Chem. Soc.* **2011**, *133*, 6914−6917.

(37) Ertl, G. Self-Organization in Reactions at Surfaces. *Surf. Sci.* **1993**, *287−288*, 1−11.

(38) Oh, S.; Eickel, C. Influence of Metal Particle Size and Support on the Catalytic Properties of Supported Rhodium: CO-$O_2$ and CO-NO Reactions. *J. Catal.* **1991**, *128*, 526−536.

(39) Ladas, S.; Poppa, H.; Boudart, M. The Adsorption and Catalytic Oxidation of Carbon Monoxide on Evaporated Palladium Particles. *Surf. Sci.* **1981**, *102*, 151−171.

(40) Iglesia, E. Design, Synthesis and Use of Cobalt-Based Fischer−Tropsch Synthesis Catalysts. *Appl. Catal., A* **1997**, *161*, 59−78.

(41) Burch, R.; Shestov, A.; Sullivan, J. A Transient Kinetic Study of the Mechanism of the NO+$H_2$ Reaction over Pt/$SiO_2$ Catalysts 1. Isotopic Transient Kinetics and Temperature Programmed Analysis. *J. Catal.* **1999**, *186*, 353−361.

(42) Dhainaut, F.; Pietrzyk, S.; Granger, P. Kinetic Investigation of the NO Reduction by $H_2$ over Noble Metal Based Catalysts. *Catal. Today* **2007**, *119*, 94−99.

(43) Hecker, W.; Bell, A. Reduction of NO by $H_2$ over Silica-Supported Rhodium: Infrared and Kinetic Studies. *J. Catal.* **1985**, *92*, 247−259.

(44) Den Breejen, J.; Radstake, P.; Bezemer, G.; Bitter, J.; Frøseth, V.; Holmen, A.; de Jong, K. On the Origin of the Cobalt Particle Size Effects in Fischer−Tropsch Catalysis. *J. Am. Chem. Soc.* **2009**, *131*, 7197−7203.

(45) Dixit, R.; Tavlarides, L. Kinetics of the Fischer−Tropsch Synthesis. *Ind. Eng. Chem. Process Des. Dev.* **1983**, *22*, 1−9.

(46) Yates, I.; Satterfield, C. Intrinsic Kinetics of the Fischer−Tropsch Synthesis on a Cobalt Catalyst. *Energy Fuels* **1991**, *5*, 168−173.

(47) Krishnamoorthy, S.; Tu, M.; Ojeda, M.; Pinna, D.; Iglesia, E. An Investigation of the Effects of Water on Rate and Selectivity for the Fischer−Tropsch Synthesis on Cobalt-Based Catalysts. *J. Catal.* **2002**, *211*, 422−433.

(48) Carballo, J.; Yang, J.; Holmen, A.; García-Rodríguez, S.; Rojas, S.; Ojeda, M.; Fierro, J. Catalytic Effects of Ruthenium Particle Size on the Fischer−Tropsch Synthesis. *J. Catal.* **2011**, *284*, 102−108.

(49) Li, J.; Jacobs, G.; Das, T.; Zhang, Y.; Davis, B. Fischer−Tropsch Synthesis: Effect of Water on the Catalytic Properties of a Co/$SiO_2$ Catalyst. *Appl. Catal., A* **2002**, *236*, 67−76.

(50) Hoffman, B.; Lukoyanov, D.; Dean, D.; Seefeldt, L. Nitrogenase: A Draft Mechanism. *Acc. Chem. Res.* **2013**, *46*, 587−595.

(51) Hibbitts, D.; Iglesia, E. Unpublished results.